

## ON THE MORPHOLOGICAL, ELECTRICAL AND PHOTOELECTRICAL PROPERTIES OF P3HT:F-SWCNTs BASED PHOTOVOLTAIC CELLS

J. AL-ZANGANAWEE<sup>a,b</sup>, S. IFTIMIE<sup>c</sup>, A. PANTAZI<sup>a,c</sup>, O. BRINCOVEANU<sup>a,c</sup>,  
R. MESTERCA<sup>a</sup>, A. RADU<sup>c</sup>, S. ANTOHE<sup>c,d</sup>, M. ENACHESCU<sup>a,d,\*</sup>

<sup>a</sup>*Center for Surface Science and Nanotechnology (CSSNT), University Politehnica of Bucharest, Romania*

<sup>b</sup>*Physics Department, College of Science, University of Diyala, Iraq*

<sup>c</sup>*University of Bucharest, Faculty of Physics, Bucharest, Romania*

<sup>d</sup>*Academy of Romanian Scientists, Bucharest, Romania*

In this study, experimental results related to the surface morphology, and photoelectrical and electrical properties of solar cells based on conductive polymer P3HT and functionalized SWCNTs are presented. The surface morphology of P3HT:F-SWCNTs photoactive layers with three different ratios (99:1, 97:3, and 94:6.0 wt., %) of P3HT:F-SWCNTs, was analyzed and an increase of root mean square roughness values with the increase of added F-SWCNTs percentage was observed. The current-voltage (I-V) curves acquired in dark conditions showed a good diode behavior for all fabricated solar cells, with relatively small values of saturation current for solar cells structures based on the P3HT:F-SWCNTs (97:3) and P3HT:F-SWCNTs (94:6) photoactive layers. The action spectra measurements of prepared solar cells samples were drawn and discussed taking into account the induced changes of added weight percentage of F-SWCNTs in photoactive layer.

(Received November 1, 2016; Accepted March 20, 2017)

*Keywords: SWCNTs, P3HT, ZnO, Solar cells*

### 1. Introduction

In the last decade, regio-regular polymer:fullerene derivatives based photovoltaic cells attracted much interest from scientific community because are easy made and relatively cheap structures, compared with silicon technology. Despite the optimization efforts, their major problems like time stability and small values of power conversion efficiency are not fully solved [1-3]. The use of carbon nanotubes (CNTs) in the architecture of organic photovoltaic cells (OPV) can be a solution to increase charge carriers' collection to electrodes which increases the overall device performances [4-6]. A special attention was paid to single wall carbon nanotubes (SWCNTs) used either as constitutive of active layer or instead of indium tin oxide (ITO) as transparent conductive film [7-9]. Thus, SWCNTs semiconducting type are usually preferred instead of metallic ones in order to avoid short-circuits or recombination [10,11]. With work function in 4.5 – 5.1 eV range, close to the valence band of most used regio-regular polymers, SWCNTs can replace fullerene derivatives from the architecture of photovoltaic structures, behaving as acceptors. Moreover, for regio-regular polymer:SWCNTs mixture the electrical mobility is increased because SWCNTs behave as exciton dissociation and hopping center for holes transport [12].

In this paper, we studied the surface morphology and the photoelectrical and electrical behavior studies of solar cells based on the P3HT:F-SWCNTs photoactive layers with different mass concentration ratios (99:1, 97:3, and 94:6 wt., %) of P3HT:F-SWCNTs blends, fabricated in ambient atmosphere using spin coating method.

---

\*Corresponding author: marius.enachescu@upb.ro

## 2. Experimental procedures

### 2.1. Materials

A mixture of 75-78% semiconducting type and 22-25% metallic type of single wall carbon nanotubes with ~70% purity and 0.3-4  $\mu\text{m}$  length was functionalized using a mild concentration solution of 6M nitric acid, used as electron acceptor material. Transparent indium tin oxide (ITO) coated glass with resistivity in the 8 – 12  $\Omega/\text{square}$  range was used as substrate. PEDOT:PSS, conductive polymer P3HT and ZnO nanoparticles ink with particle size in the 10-15 nm range were used without any purification processes as hole transport layer, electron donor polymer, and electron transport layer materials, respectively.

### 2.2. Solar cells samples preparation

The conventional solar cell samples were prepared by spin coating, in ambient atmosphere, by customizing the photoactive layer as a blend between the conductive polymer P3HT and functionalized single wall carbon nanotubes, in three different weight percentage ratios (99:1, 97:3, 94:6 wt., %). The procedure used for solar cell samples preparation is comprised from the following four steps. At first, a hole transport layer (HTL) of PEDOT:PSS material was spin-coated onto a clean ITO coated glass substrate (anode layer) and annealed at 110°C for half hour. In the second step, a mixture of P3HT:F-SWCNTs photoactive film was spin-coated onto PEDOT:PSS layer and was thermally treated at 70°C for half hour because the conductive polymer P3HT have been shown an early crystalline structure [13,14]. In the next step, an electron transport layer (ETL) of ZnO ink was deposited on top of the photoactive layer by spin coating and annealed at 110°C for half hour. Finally, a cathode layer of aluminum (Al) was deposited onto the ZnO layer using thermal evaporation method under vacuum. The schematic representation of the prepared solar cell structure and the energy level diagram of the constituent materials are shown in Figure 1a and b, respectively.

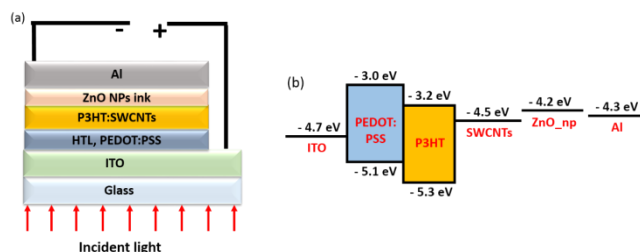


Fig. 1 (a) *The schematic representation of the prepared solar cells based on the P3HT:F-SWCNTs photoactive layer and (b) the constituent materials energy level diagram.*

### 2.3. Characterization techniques

Micro-Raman spectroscopy using a green laser with 532 nm wavelength was performed on the pure SWCNTs and F-SWCNTs. Field emission scanning electron microscopy (FESEM) and atomic force microscopy (AFM) studies were involved to determine the morphology features of the photoactive layers samples. Current-voltage (I-V) curves in dark and external quantum efficiency (EQE) measurements of all prepared samples were acquired in ambient atmosphere.

## 3. Results and discussions

The Raman spectra of the pure and functionalized SWCNTs samples are represented in Figure 2 a, and b, respectively. Three distinct regions can be distinguished in the Raman spectra of the SWCNTs, namely Radial Breathing Mode (RBM) localized in the 150  $\text{cm}^{-1}$  – 300  $\text{cm}^{-1}$  range which is characteristic to SWCNTs, D band which is related to scattering on  $sp^3$  carbon atoms and G band which is relevant to in-plane oscillations of  $sp^2$  hybridized carbon atoms from the nanotubes' architecture [15,16].

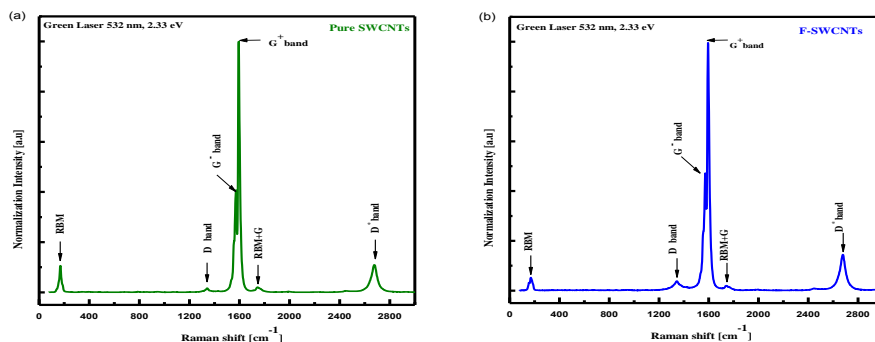


Fig. 2 (a) Pure SWCNTs and (b) functionalized SWCNTs Raman spectra.

Lorentzian fitting was applied for the low frequency RBM peaks in the Raman spectra for pure and functionalized SWCNTs in order to see the effects of the functionalization process on the intensity, Raman shift position and shape of the RBM peaks. After the nanotubes' functionalization it was observed that the intensity of the central peak was slightly decreased, while the RBM peaks' position was shifted to a higher frequency (see Figure 3 a and b) and their shape was modified as a result of the nitric acid treatment which created local defects in the structure of the nanotubes' wall due to the attachment of different functional groups.

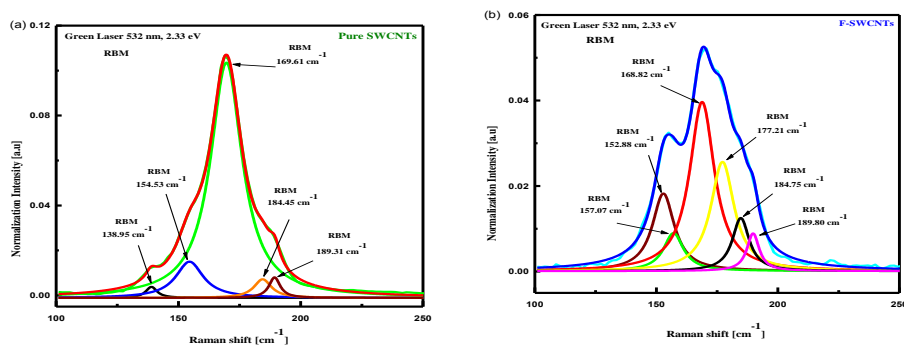


Fig. 3 Raman spectra radial breathing mode (RBM) of pristine SWCNTs and functionalized SWCNTs recorded using green laser with 532 nm wavelength and 2.33 eV energy

The D band displayed by the functionalized SWCNTs shows a higher intensity and has a higher Raman shift position compared to the D band of pure SWCNT (see Figure 3 a and b, and Table 1 and 2). Moreover, the former are broader than the latter and the increase in width can be attributed to the increase of the localized defects in the nanotubes' structure. The increase value of the  $I_D/I_G$  ratio after functionalization, where  $I_D$  and  $I_G$  correspond to the D, and G bands peaks maximum intensities, respectively, is another for this correlation.

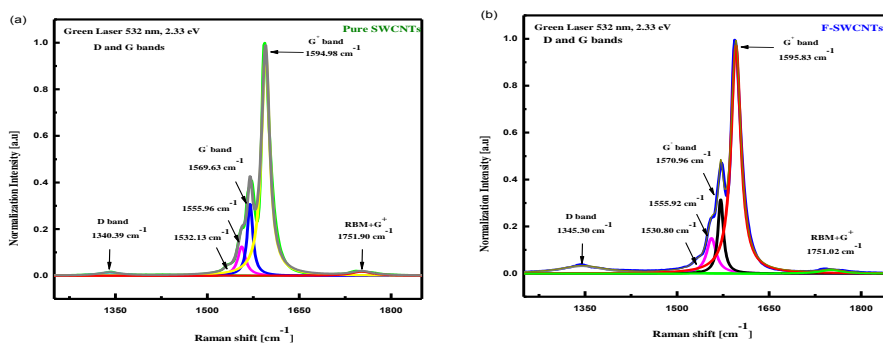


Fig. 4 D and G bands peaks of the Raman spectra for: (a) Raw SWCNTs and (b) F-SWCNTs.

Table 1 Lorentzian fitting summary of D, G<sup>-</sup>, G<sup>+</sup> peaks of Raman spectrum for SWCNTs.

Name of peak	Peak Raman Shift (cm <sup>-1</sup> )	Peak amplitude	Peak width	Peak Height
D band	1340.39	0.96	45.36	0.016
G <sup>-</sup> band	1532.13	0.16	8.03	0.013
G <sup>-</sup> band	1555.96	3.03	15.37	0.125
G <sup>-</sup> band	1569.63	5.30	10.95	0.308
G <sup>+</sup> band	1594.98	24.47	16.03	0.971

Table 2 Lorentzian fitting summary of D, G<sup>-</sup>, G<sup>+</sup> peaks of Raman spectrum for F-SWCNTs.

Name of peak	Peak Raman Shift (cm <sup>-1</sup> )	Peak amplitude	Peak width	Peak Height
D band	1345.30	4.59	89.87	0.036
G <sup>-</sup> band	1530.80	0.35	13.98	0.015
G <sup>-</sup> band	1555.92	4.49	18.89	0.15
G <sup>-</sup> band	1570.96	5.29	10.65	0.31
G <sup>+</sup> band	1595.83	29.30	19.18	0.972

Figure 5 a, b, and c illustrated the atomic force microscope topography images of P3HT:F-SWCNTs (99:1), P3HT:F-SWCNTs (97:3), and P3HT:F-SWCNTs (94:6) photoactive layers, respectively, prepared using the spin coating technique.

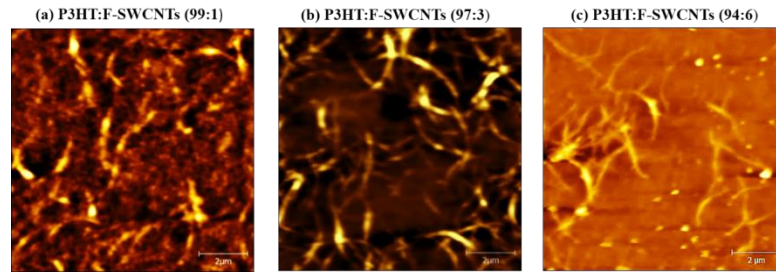


Fig. 5 Atomic force microscopy topography images of the (a) P3HT:F-SWCNTs (99:1), (b) P3HT:F-SWCNTs (97:3) and (c) P3HT:F-SWCNTs (94:6) photoactive layers that were deposited by spin-coating in ambient conditions.

With the help of an image processing software, the root mean square (RMS) roughness values illustrated in Table 3 were determined for all prepared samples to provide more insight on how the polymer:nanotubes ratio affects the surface homogeneity.

The root mean square (RMS) roughness of the surface of photoactive layer can be determine using equation 1 [17]:

$$R_{RMS} = \sqrt{\frac{1}{L} \int_0^L |Z^2(x)| dx} \quad (1)$$

Where  $R_{RMS}$  is the roughness of the surface and  $Z(x)$  is a function which gives description about the profile of the surface in expressions of height  $Z$  and position  $x$  taking into consideration the length  $L$ .

Table 3 RMS values for surface roughness for the prepared photoactive layers.

Photoactive layer composition	Surface Roughness
(a) P3HT:F-SWCNTs (99:1)	2.4 nm
(b) P3HT:F-SWCNTs (97:3)	7.1 nm
(c) P3HT:F-SWCNTs (94:6)	13.7 nm

Figure 6a, b and c show the field emission scanning electron microscopy micrographs of the synthesized photoactive layers for different P3HT : SWCNTs weight ratios.

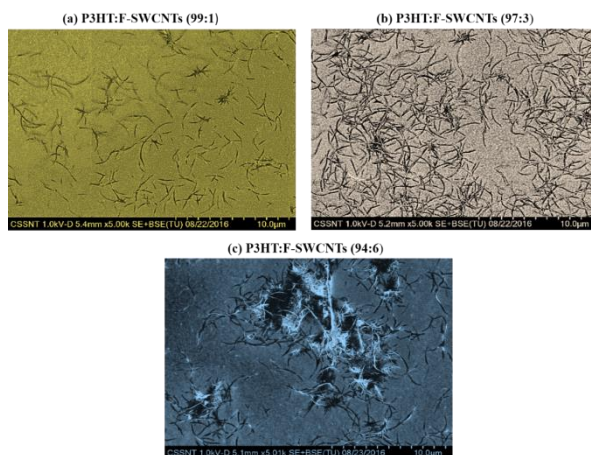


Fig. 6 FESEM morphology images of (a) P3HT:F-SWCNTs (99:1), (b) P3HT:F-SWCNTs (97:3) and (c) P3HT:F-SWCNTs (94:6) photoactive layers deposited by spin-coating in ambient conditions.

The increase in the added F-SWCNTs weight percentage has led to the increase in the RMS values most likely due to the formation of bundles, mostly in the case of P3HT:F-SWCNTs (94:6) photoactive layer where the AFM image and FESEM micrographs showed that the formed bundles were pushed onto the surface.

By their superior electric conductivity compared with conductive polymers, SWCNTs improve the overall electric properties of solar cell devices photoactive layer. Furthermore, by the attachment of various functional chemical groups to the SWCNTs backbone the charge carriers' collection to solar cells electrode is highly facilitated. Nevertheless, an amount in excess can lead to short-circuits if the carbon nanotubes lengths become comparable with the thickness of the photoactive layer [18-20], and, also, can be pushed to the surface of the photoactive layer. In this context, an optimal amount should be established in order to improve the solar cell performances of fabricated devices and to avoid their collapse. For our fabricated solar cell samples, the P3HT:F-SWCNTs (97:3.0) active layer looks to be more homogenous and to have a more uniform distribution of SWCNTs than P3HT:F-SWCNTs (99:1.0), and P3HT:F-SWCNTs (94:6.0) photoactive layers, respectively, as was observed by field emission electron microscopy analysis.

The current-voltage curves obtained for the fabricated solar cells sample for both reverse and forward voltage bias are illustrated in Figure 7. All measurements were acquired in dark and in ambient atmosphere. All I-V dark characteristics display a non-linear behavior and high asymmetry as a consequence of an blocking contact at the interface between the ITO anode layer, PEDOT:PSS hole transport layer and the photoactive layer interface. However, the photoactive layer/ZnO electron transport layer/Al cathode layer structure has an Ohmic behavior [21]. The diode quality factor ( $p$ ) and the dark saturation current ( $I_s$ ) were calculated for all prepared structures to assess the influence of the filler's added mass on the electrical behavior of the prepared solar cells structures and are indicated in Table 4.

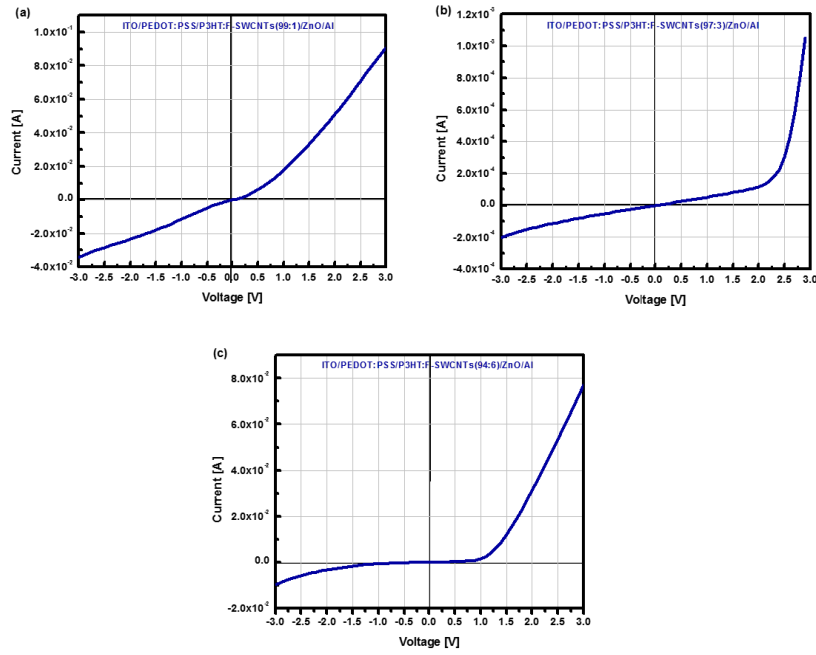


Fig. 7 Current-Voltage curves in dark of the solar cells structures (ITO/PEDOT:PSS/P3HT:F-SWCNTs/ZnO/Al) with different photoactive layer mass concentrations ratio of P3HT: SWCNTs (a) P3HT:F-SWCNTs (99:1), (b) P3HT:F-SWCNTs (97:3) and (c) P3HT:F-SWCNTs (94:6).

Table 4 The calculated values of the ideality factor ( $p$ ) and the saturation current ( $I_s$ ) of fabricated solar cell structures samples

OPV structures samples	Ideality factor $P$	Saturation current $I_s$ (mA)
(a) ITO/ PEDOT/ P3HT:F-SWCNTs (99:1)/ZnO/Al	0.6	1.5
(b) ITO/PEDOT/ P3HT:F-SWCNTs (97:3)/ZnO/Al	0.8	$12 \times 10^{-3}$
(c) ITO/PEDOT/ P3HT:F-SWCNTs (94:6) /ZnO/Al	1.5	$122 \times 10^{-6}$

Taking into account an ideal diode, the mathematical relationship between the total current flowing through diode ( $I$ ) and the dark saturation current ( $I_s$ ) is given by:

$$I = I_s \left[ \exp\left(\frac{qV}{k_B T}\right) - 1 \right] \quad (2)$$

Where  $V$ ,  $q$ ,  $k_B$ , and  $T$  are the applied voltage, elementary charge, Boltzmann constant and the absolute temperature, respectively. In the case of real diodes, the expression (2) becomes:

$$I = I_s \left[ \exp\left(\frac{qV}{p k_B T}\right) - 1 \right] \quad (3)$$

In the equation (3),  $p$  is the ideality factor, a number that has values in 1-2 domain, and is associated with material quality. Also, it gives a measure of devices electric behavior being inversely proportional to the total current through diode. Big values of ideality factor leads to big values of dark saturation current which is a measure of high recombination [22].

For ITO/PEDOT/P3HT:F-SWCNTs (97:3)/ZnO/Al solar cell structure, the ideality factor was closer to one than for the other prepared samples ( $p = 0.8$ ) indicating a better diode behavior.

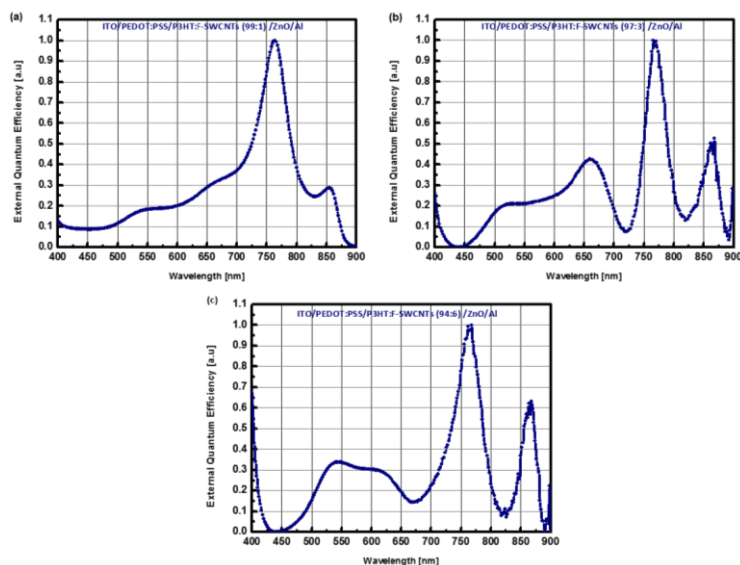


Fig. 8 The action spectra of solar cells structures (ITO/PEDOT:PSS/P3HT:F-SWCNTs/ZnO/Al) with different photoactive layer mass concentrations ratio of P3HT: SWCNTs (a) P3HT:F-SWCNTs (99:1), (b) P3HT:F-SWCNTs (97:3) and (c) P3HT:F-SWCNTs (94:6).

The action spectra of prepared solar cells samples are shown in Figure 8a, b and c. The measurements of the photoelectrical properties for all samples were carried out in ambient atmosphere. From Figure 8, we calculated the highest values of the external quantum efficiency (EQE) of synthesized solar cell samples (see Table 5). The highest calculated value of EQE was 15% for the prepared solar cell samples based on the P3HT:F-SWCNTs (97:3.0) composition of the photoactive layer (see Table 3).

Table 5 The external quantum efficiency (EQE) highest calculated values of prepared solar cell structures samples

Solar cell structures	EQE
(a) ITO/ PEDOT/ P3HT:F-SWCNTs (99:1)/ZnO/Al	5%
(b) ITO/PEDOT/ P3HT:F-SWCNTs (97:3)/ZnO/Al	15%
(c) ITO/PEDOT/ P3HT:F-SWCNTs (94:6)/ZnO/Al	12%

Figure 8(a) showed that the contribution of P3HT conductive polymer is not clearly seen in the external quantum efficiency diagram of the solar cell structure based on the P3HT:F-SWCNTs (99:1) photoactive layer, most likely because of the good attachment of polymer P3HT functional groups to the walls and ends of SWCNTs. By increasing the weight percentage ratio of carbon nanotubes in the photoactive layer, the contribution of the specific absorption of polymer in the 500-650 nm wavelength range of the external quantum efficiency becomes significant (see figure 8 b), and it very clearly can be seen in the case of the solar cell structure based on the P3HT:F-SWCNTs (94:6) due to the formation of bundles by increasing carbon nanotubes weight percentage in the photoactive layer (see figure 8c).

Despite their relatively good diode behavior, in order to optimize the overall performances of such photovoltaic devices, some more studies are strongly required.

#### 4. Conclusions

Solar cell structures based on the blends of P3HT conductive polymer and F-SWCNTs were made using spin-coating, in ambient atmosphere. The photoactive layer composition mass

ratios of P3HT:F-SWCNTs were 99:1.0, 97:3.0, and 94:6.0 wt., %. The AFM images analysis of the photoactive layers confirmed that by increasing the mass concentration ratio of SWCNTs into P3HT polymer film leads to increase of the roughness of the surface. Furthermore, the AFM and SEM images analysis for P3HT:F-SWCNTs (94:6.0) photoactive film showed that the bundles of carbon nanotubes were agglomerated and some of them were pushed up to the film surface. The current-voltage measurements in dark for all prepared solar cells samples showed that the best diode behaviour was for the solar cell structure based on the P3HT:F-SWCNTs (97:3) photoactive layer. The results from the external quantum efficiency measurements for prepared solar cells samples showed good attachment between P3HT functional groups and walls of F-SWCNTs for ITO/PEDOT:PSS/P3HT:F-SWCNTs (99:1.0)/ZnO/Al structures.

### Acknowledgements

This work was supported by Romanian Ministry of Education and Scientific Research and by Executive Agency for Higher Education, Research, Development and Innovation, under Projects PCCA 2-66/2014 and ENIAC 04/2014. J. Al-Zanganawee acknowledges the support of the Ministry of Higher Education and Scientific Research of Iraq.

### References

- [1] C.J. Brabec, N.S. Sariciftci, J.C. Hummelen, *Advanced Functional Materials* **11**, 15 (2001)
- [2] G. Li, V. Shrotriya, J. Huang, Y. Yao, T. Moriarty, K. Emery, Y. Yang, *Nature Materials* **4**, 864 (2005)
- [3] S. Iftimie, A. Radu, M. Radu, C. Besleaga, I. Pana, S. Craciun, M. Girtan, L. Ion, S. Antohe, *Digest Journal of Nanomaterials and Biostructures* **6**, 1631 (2011)
- [4] E. Kymakis, G.A.J. Amaratunga, *Applied Physics Letters* **80**, 112 (2002)
- [5] L. Liu, W.E. Stanchina, G. Li, *Applied Physics Letters* **94**, 233309 (2009)
- [6] S. Berson, R. de Bettignies, S. Bailly, S. Guillerez, B. Jusselme, *Advanced Functional Material* **17**, 3363 (2007)
- [7] E. Kyamakis, E. Stratakis, E. Koudoumas, *Thin Solid Films* **515**, 8598 (2007)
- [8] M. W. Rowell, M.A. Topinka, M.D. McGehee, H.J. Prall, G. Denneler, N.S. Sariciftci, L. Hu, G. Gruner, *Applied Physics Letters* **88**, 233506 (2006)
- [9] V. Sgobba, D.M. Guldi, *Journal of Materials Chemistry* **18**, 153 (2008)
- [10] N.J. Alley, K.-S. Liao, E. Andreoli, S. Dias, E.P. Dillon, A.W. Orbaek, A.R. Barron, H.J. Byrne, S.A. Curran, *Synthetic Metals* **162**, 95 (2012)
- [11] H. Derbal-Habak, C. Bergeret, J. Cousseau, J.M. Nunzi, *Solar Energy Materials & Solar Cells* **95**, S53 (2011)
- [12] B. Pradhan, S.K. Batabyal, A.J. Pal, *Applied Physics Letters* **88**, 093106 (2006)
- [13] J. Al-Zanganawee, M. Al-Timmi, A. Pantazi, O. Brincoveanu, C. Moise, R. Mesterca, D. Balan, S. Iftimie, M. Enachescu, *Journal of Ovonic Research* **12**, 201 (2016)
- [14] A. Radu, S. Iftimie, V. Ghenescu, C. Besleaga, V.A. Antohe, G. Bratina, L. Ion, S. Craciun, M. Girtan, S. Antohe, *Digest Journal of Nanomaterials and Biostructures* **3**, 1141 (2011)
- [15] M.S. Dresselhaus, P.C. Eklund, *Advances in Physics* **49**, 705 (2000)
- [16] P.C. Eklund, J.M. Holden, R.A. Jishi, *Carbon* **33**, 959 (1995)
- [17] E.S. Gadelmawla, M.M. Koura, T.M.A. Maksoud, I.M. Elewa, H.H. Soliman, *Journal of Materials Processing Technology* **123**, 133 (2002)
- [18] L. Fen, Z. Dewei, S. Junling, C. Jing, T. Swee, K. Lin, D. Hilmi, S. Handong, S. Xiao, *Journal of Modern Optics* **61**, 21 (2014)
- [19] J. Kumar, R.K. Singh, V. Kumar, R.C. Rastogi, R. Singh, *Diamond and Related Materials* **16**, 446 (2007)
- [20] W. Zhang, T.M. Swager, *Journal of the American Chemical Society* **129**, 7714 (2007)
- [21] L. Magherusan, P. Skraba, C. Besleaga, S. Iftimie, N. Dina, M. Bulgariu, C.-G. Bostan, C. Tazlaonu, A. Radu, L. Ion, M. Radu, A. Tanase, G. Bratina, S. Antohe, *J. Optoelectron. Adv. M.* **12**, 212 (2010)
- [22] S. Antohe, V. Ruxandra, L. Tugulea, V. Gheorghe, D. Ionaşcu, *Journal de Physique III France* **6**, 1133 (1996)